Polarized neutron scattering and x-ray magnetic circular dichroism studies of the heavy-fermion superconductor UNi_2Al_3

2000 J. Phys.: Condens. Matter 12 7857

(http://iopscience.iop.org/0953-8984/12/36/301)

J. Phys.: Condens. Matter **12** (2000) 7857–7867. Printed in the UK PII: S0953-8984(00)11906-X

Polarized neutron scattering and x-ray magnetic circular dichroism studies of the heavy-fermion superconductor UNi_2Al_3

N Kernavanois†, J-X Boucherle†¶, P Dalmas de Réotier†, F Givord†¶, E Lelièvre-Berna‡, E Ressouche†, A Rogalev§, J-P Sanchez†, N Sato‖ and A Yaouanc†

† Commissariat à l'Energie Atomique, Département de Recherche Fondamentale sur la Matière Condensée, F-38054 Grenoble Cédex 9, France
‡ Institut Laue–Langevin, BP 156, F-38042 Grenoble Cédex 9, France
§ European Synchrotron Radiation Facility, BP 220, F-38043 Grenoble Cédex, France
‖ Department of Physics, Faculty of Science, Tohoku University, Sendai 980-77, Japan

Received 16 February 2000, in final form 21 June 2000

Abstract. A polarized neutron scattering experiment and an x-ray magnetic circular dichroism (XMCD) study at the $M_{4,5}$ edges of uranium have been performed on a single crystal of the heavy-fermion superconductor UNi_2Al_3 in the paramagnetic phase. Projections of the maximum-entropy reconstructions of the magnetization distribution obtained from neutron data evidence a large and almost spherical distribution on the U sites and an induced moment at the Ni sites. Refinements of the magnetic structure factors within the dipolar approximation allow one to quantify the Ni contribution and the orbital and spin uranium moments, and reveal a diffuse contribution parallel to the 5f moment. The XMCD study leads to a value of the 5f orbital contribution in agreement with the neutron one. For both neutron and XMCD experiments, we compare our results with previous measurements performed on the parent compound UPd_2Al_3.

1. Introduction

Coexistence on a microscopic scale of superconductivity with a long-range antiferromagnetic order in the heavy-fermion superconductors (HFS) is an important issue in the physics of strongly correlated electron systems. One of the main areas of interest focuses on the interplay between magnetism and superconductivity [1, 2]. In order to elucidate the nature of HFS, comparison between several representatives and a deeper understanding of the 5f-electron nature are of first importance. Indeed, 5f hydridization with d and conduction electron bands could explain the enhanced density of states at the Fermi level derived from the large Sommerfeld coefficients (low-temperature electronic coefficients of the specific heat, γ) observed for uranium HFS.

The superconducting and magnetic properties of UNi_2Al_3 are not so well documented compared to those of UPd_2Al_3 owing to the difficulties of preparing good single crystals. Nevertheless, the analysis of the susceptibility and specific heat measurements indicates typical behaviour of a transition from localized to weakly delocalized 5f electrons at relatively high temperature [3,4] in both cases and suggests a tetravalent ($5f^2$) uranium state [4,5]. But whereas

¶ CNRS staff.

0953-8984/00/367857+11$30.00

there are substantial similarities (table 1) in their macroscopic properties, several indications lead one to anticipate different hybridization behaviour in these two parent compounds:

(i) A shift toward higher temperatures of the maxima of both the resistivity and the susceptibility is observed together with the decrease of the magnetic ordering temperature T_N, the superconducting temperature T_c, the antiferromagnetic moment and the smaller entropy released at T_N when replacing Pd by Ni, suggesting a stronger interaction between 5f electrons and conduction electrons in UNi_2Al_3 than in UPd_2Al_3 [6].

(ii) Electronic band-structure calculations using the local density approximation (LDA) show that the $(T–U)_d$ bands in UT_2Al_3, with T = Ni and Pd, are centred respectively at −2 eV and −4 eV below the Fermi energy [7–9]. This feature causes a larger U_{5f} band in UNi_2Al_3 through stronger Ni_{3d}–U_{5f} hybridization, which is expected to induce a magnetization density at the Ni sites.

As a previous magnetization density measurement performed on UPd_2Al_3 [10] evidenced no moment on the Pd sites, we decided to probe the Ni magnetization in UNi_2Al_3.

Table 1. Comparison of the physical properties for UNi_2Al_3 and UPd_2Al_3. a and c are the lattice parameters at room temperature, γ is the Sommerfeld coefficient deduced from specific heat measurements, T_N the Néel temperature and T_c the superconducting temperature [3, 11]. μ_{AF} is the uranium magnetic moment in the normal antiferromagnetic (AF) state deduced from neutron scattering data [12].

UT_2Al_3	Space group	a (Å)	c (Å)	γ (mJ mol^{-1} K^{-2})	T_N (K)	T_c (K)	μ_{AF} (μ_B)
T = Ni	$P6/mmm$	5.207	4.018	120	4.6	1	0.2
T = Pd	$P6/mmm$	5.365	4.186	150	14	2	0.85

This paper is divided into four parts. We first present the neutron scattering experiments and results. The following section is devoted to the x-ray magnetic circular dichroism (XMCD) study. Results are then discussed and compared with those from previous experiments performed on the parent compound UPd_2Al_3. Conclusions are drawn in section 5.

All the experiments presented in this paper have been carried out with the same single crystal of UNi_2Al_3 (∼4 mm in diameter and ∼4 mm in height) prepared at Sendai. It has been grown by the Czochralski method, using the same procedure as described in reference [13].

2. Determination of the magnetization distribution of UNi_2Al_3 by means of polarized neutron scattering

The classical polarized beam technique (flipping ratio method) [14] takes advantage of the interference between the magnetic and nuclear signals. Its sensitivity to small magnetic moments is greater than that of the conventional unpolarized beam method. This technique consists in measuring the ratio between the intensities I^+ and I^- of a Bragg reflection, for an incident polarization $\boldsymbol{p}$ of the beam respectively parallel (+) and antiparallel (−) to the applied field direction ($\boldsymbol{z}$). This ratio, called the flipping ratio, can be written for a centrosymmetric structure as

$$R = \frac{I^+}{I^-} = \frac{1 + 2pq^2\gamma + q^2\gamma^2}{1 - 2pq^2\gamma + q^2\gamma^2} \tag{1}$$

with $q^2 = \sin^2\alpha$, α being the angle between the scattering vector and the $\boldsymbol{z}$-direction and $\gamma = F_M/F_N$ the ratio of the magnetic and nuclear structure factors. If F_N is known, the

measurement of R and thus of γ gives the value of F_M in both sign and amplitude. Very precise nuclear structure factors and a good knowledge of the extinction effect in the sample are then necessary to analyse polarized neutron data. Therefore a preliminary unpolarized neutron experiment has been carried out to determine the nuclear parameters under the same experimental conditions as were used for the polarized experiment. They correspond to a broad maximum in the magnetic susceptibility of UNi_2Al_3 [13], with an induced magnetic moment per formula unit in our sample of $\mu^{\text{bulk}} \simeq 47.0(5) \times 10^{-3}\ \mu_B$ at 100 K and under a field of 4.6 T applied along the crystallographic a-axis.

2.1. Nuclear structure refinement

The unpolarized neutron experiment has been performed on the Collaborating Research Group (CRG) D15 instrument of the Institut Laue–Langevin (ILL, France) using a wavelength $\lambda = 0.855$ Å at a temperature $T = 100$ K. To check whether the applied field used in the polarized neutron experiment could modify the extinction strength, two measurements were performed in fields of $B_{\text{ext}} = 0$ T and $B_{\text{ext}} = 4.6$ T. They led to the same results. 473 reflections were collected for both cases in the normal beam geometry (mainly in the ($\boldsymbol{b}^\star$, $\boldsymbol{c}^\star$) plane), leading to a set of 385 independent reflections. The experimental data were corrected for the absorption (linear absorption coefficient $\mu = 0.0183$ mm^{-1}). This experiment confirmed the already-reported hexagonal structure of UNi_2Al_3 [3]. At 100 K the cell parameters are $a = 5.197(1)$ Å and $c = 4.013(1)$ Å. The structure parameters were then refined using the program MXD [15], including a Becker–Coppens correction for the extinction [16]. This extinction correction turned out to be rather important (nearly a factor of 2 for a few reflections), due to both the good quality and the large size of the sample. Results are presented in table 2 and a view of the unit cell is shown in figure 1. We also checked the possible mixing between Ni and Al atoms at their sites, which turned out to be negligible ($\lesssim$0.7%).

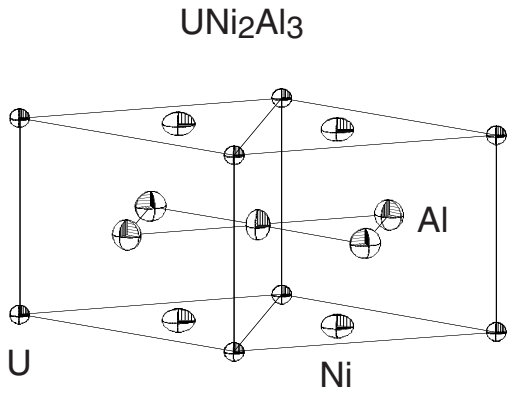

Figure 1. A view of the UNi_2Al_3 structure at 100 K with the thermal motion ellipsoids.

2.2. Polarized neutron measurements

The flipping ratio measurements were performed on the polarized hot-neutron diffractometer D3 of the ILL, mainly using a wavelength $\lambda = 0.711$ Å (with a corresponding polarization of the incident beam $p \simeq 0.93$) provided by a Heusler monochromator with an appropriate resonant harmonic filter to remove the $\lambda/2$ contamination. The experimental conditions were $T = 100$ K and $B_{\text{ext}} = 4.6$ T. 185 flipping ratios, reduced to a set of 33 independent measurements after

Table 2. Atomic positions, thermal anisotropic factors U_{ij} and equivalent thermal isotropic factors B_{equi} for UNi_2Al_3 deduced from neutron scattering at 100 K. Refinement leads to a $\chi^2 = 3.51$ and a weighted residual factor of

$$R_\omega(F^2) = \sqrt{\sum[(I_{\text{obs}} - I_{\text{calc}})/\sigma_{I_{\text{obs}}}]^2 \Big/ \sum[I_{\text{obs}}/\sigma_{I_{\text{obs}}}]^2} = 5.62\%$$

where I_{obs} and I_{calc} are the observed and calculated intensities respectively and $\sigma_{I_{\text{obs}}}$ is the standard deviation. The mosaicity of the crystal is $\eta = 0.63(1)'$ corresponding to an extinction coefficient $g = 1540(30)$ rad^{-1} ($\eta = 1/(2\sqrt{\pi}g)$).

Atomic species	Atomic sites	Atomic positions	U_{ij}			B_{equi}
U	1a	(0, 0, 0)	$U_{11} = 0.00126(7)$ $U_{22} = U_{11}$ $U_{33} = 0.00098(8)$	$U_{12} = U_{11}/2$ $U_{23} = 0$	$U_{13} = 0$	$B_{\text{U}} = 0.09(1)$
Ni	2c	$(\frac{1}{3}, \frac{2}{3}, 0)$	$U_{11} = 0.00345(6)$ $U_{22} = U_{11}$ $U_{33} = 0.00148(7)$	$U_{12} = U_{11}/2$ $U_{23} = 0$	$U_{13} = 0$	$B_{\text{Ni}} = 0.22(1)$
Al	3g	$(\frac{1}{2}, 0, \frac{1}{2})$	$U_{11} = 0.00289(11)$ $U_{22} = 0.00185(14)$ $U_{33} = 0.00260(9)$	$U_{12} = U_{22}/2$ $U_{23} = 0$	$U_{13} = 0$	$B_{\text{Al}} = 0.19(1)$

averaging over equivalent reflections, were collected up to $(\sin\theta)/\lambda = 0.9$ Å^{-1}. In addition and owing to the large extinction effect observed on D15, flipping ratios of some particular reflections were measured at two additional short wavelengths $\lambda = 0.420$ and 0.545 Å ($p \simeq 0.85$ and 0.90, respectively). The extinction coefficient deduced from these measurements turned out to be in perfect agreement with the one obtained from the D15 integrated intensities, showing that the extinction correction was appropriate for further treatments.

2.3. Results

The experiment provides the magnetic structure factors $F_M(h, k, l)$, which are the Fourier components of the magnetization distribution. Two different methods of analysis have been used:

(i) *Fourier analysis using the three-dimensional maximum entropy (MaxEnt) technique.* This method gives the most probable magnetization distribution map compatible with the measured structure factors, given the experimental uncertainties. This map is selected with the help of an *a priori* assumption about the probability for a given point to carry a magnetization. The usual assumption is that all of the points have the same probability (uniform distribution hypothesis); however, prior knowledge can be introduced in the procedure through non-uniform distributions [17–19]. The main advantage of the MaxEnt technique, compared to the classical Fourier synthesis, is that it makes no assumption concerning unmeasured Fourier components and takes into account experimental uncertainties.

Figure 2 shows the projections for UNi_2Al_3 of the magnetization distribution along the $\boldsymbol{a}$- and $\boldsymbol{c}$-axes, respectively, using the uniform distribution hypothesis and fixing the (0, 0, 0) component to the μ^{bulk}-value. In the two maps, we can notice that, whereas most of the magnetization is localized on the uranium sites, a small contribution is observed at the Ni positions. To check this result, we performed further calculations using non-uniform distributions with magnetization on the U sites only. All of these attempts confirmed the density found on the Ni atoms.

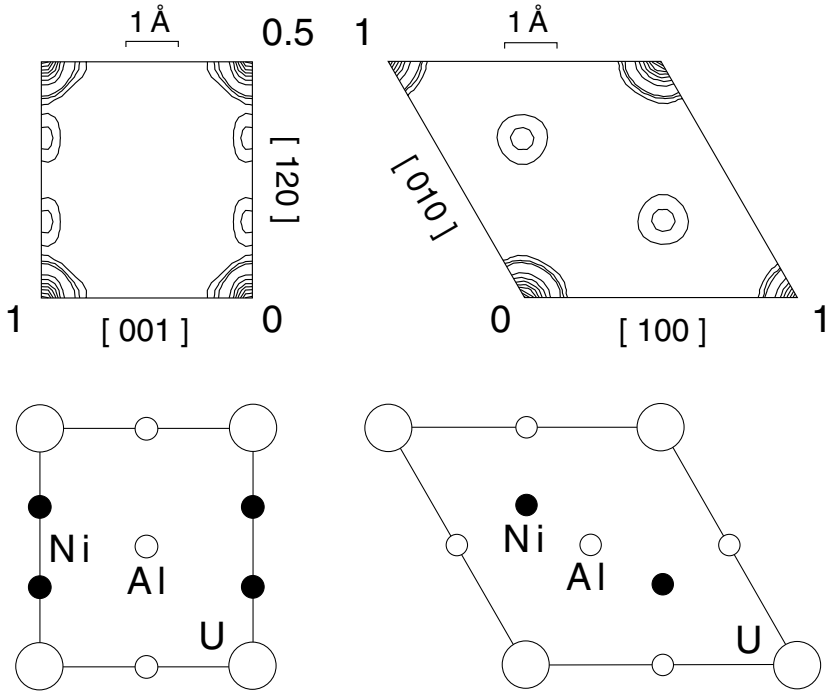

Figure 2. Magnetization distribution projections for UNi_2Al_3 along the $\boldsymbol{a}$-axis (left-hand panel) and the $\boldsymbol{c}$-axis (right-hand panel). The contour lines are from 1×10^{-3} μ_B Å^{-2} up to 73×10^{-3} μ_B Å^{-2} (83×10^{-3} μ_B Å^{-2}) along the $\boldsymbol{a}$-direction ($\boldsymbol{c}$-direction) near the uranium site with a separation between the contour lines of 1×10^{-3} μ_B Å^{-2} for the three lowest ones (far from the uranium centre) and 1×10^{-2} μ_B Å^{-2} elsewhere. Near the Ni sites, the contour lines are at 1 and 2×10^{-3} μ_B Å^{-2}.

(ii) *Model refinement*. In order to quantify the magnetic contributions, we performed least-squares refinements of the experimental magnetic structure factors within the dipolar approximation [20], i.e. just considering the isotropic term in the development of the form factor. On the U site the form factor was thus written as $f^{\mathrm{U}}(h,k,l) = \langle j_0 \rangle + C_2 \langle j_2 \rangle$, whereas for the Ni site, only the $\langle j_0 \rangle$ term has been taken into account since no orbital contribution is expected. In these expressions, $\langle j_0 \rangle$ and $\langle j_2 \rangle$ are the radial integrals tabulated in reference [21] for each element valency, and C_2 is the ratio of the orbital to the total uranium magnetic moment. The magnetic structure factor is simply

$$F_M(h,k,l) = \sum_{i \text{ atoms}} \mu^i f^i(h,k,l) \mathrm{e}^{2\pi \mathrm{i}(hx_i + ky_i + lz_i)} \tag{2}$$

where μ^i is the total magnetic moment on atom i and (x_i, y_i, z_i) its coordinates. Such a refinement allows the determination of the total magnetic contributions on uranium and nickel together with the C_2-value of the uranium.

Two different fits have been performed for U^{4+} and U^{3+} (Ni^0 (metal) in each case) with the MAGLSQ program [22]. They turned out to be equivalent and roughly lead to the same conclusions. The results are reported in table 3. The linear behaviour of the magnetization with an applied field up to 10 T has been checked and, to allow a direct comparison with XMCD results, all the magnetic moments are thus expressed as susceptibilities. This convention will be used throughout this paper.

Table 3. Summary of the different results obtained from susceptibility measurements, polarized neutron scattering and XMCD for both UNi_2Al_3 and UPd_2Al_3. $\mu^{\rm bulk}$ is the magnetic moment per formula unit. Magnetic moments are expressed as susceptibilities in $10^{-3}\ \mu_B\ T^{-1}$ and the effective spins in T^{-1}. The UPd_2Al_3 results are taken from [10] and [31]; the free-ion values are from [34].

	T = Ni		T = Pd	
UT_2Al_3	U^{4+}	U^{3+}	U^{4+}	U^{3+}
Susceptibility measurements:				
$\mu^{\rm bulk}$	10.2(1)	10.2(1)	32.2(2)	32.2(2)
Neutron experiments:				
$\mu^{\rm U}$	8.80(6)	8.65(6)	28.4(8)	28.0(8)
$\mu^{\rm T}$	0.35(4)	0.35(4)	0	0
C_2	1.49(6)	1.67(6)	1.78(19)	1.99(24)
χ^2	1.27	1.36	0.614	0.608
Deduced values				
$\mu^{\rm neut} = \mu^{\rm U} + 2\mu^{\rm T}$	9.50(10)	9.35(10)	28.4(8)	28.0(8)
$\mu^{\rm cond} = \mu^{\rm bulk} - \mu^{\rm neut}$	0.70(14)	0.85(14)	3.8(8)	4.2(8)
$\Re_L \equiv -\mu_L^{\rm U}/\mu_S^{\rm U} = C_2/(C_2-1)$	3.04(25)	2.49(13)	2.28(32)	2.01(25)
$\mu_L^{\rm U} = C_2\mu^{\rm U}$	13.11(54)	14.44(53)	50.6(5.7)	55.7(7.0)
$\mu_S^{\rm U} = \mu^{\rm U} - \mu_L^{\rm U}$	−4.31(54)	−5.75(53)	−22.2(5.8)	−27.7(7.0)
XMCD experiments:				
n_h	12	11	12	11
$\mu_L^{\rm U}$	13(1.8)	12(1.7)	64.0(4.4)	58.6(4.0)
$\langle S_z^e \rangle$	0.0098(12)	0.0090(10)	0.054(4)	0.049(4)
Deduced values				
$\Re_T \equiv \langle T_z \rangle / \langle S_z \rangle$	1.22(65)	1.46(92)	0.67(15)	0.74(17)
Free-ion values				
C_2	1.43	1.64	1.43	1.64
$\Re_L^{\rm i.c.}$	3.34	2.55	3.34	2.55
$\Re_T^{\rm i.c.}$	1.15	0.57	1.15	0.57

Figure 3 shows the comparison of observed/calculated magnetic structure factors for the U^{4+} configuration. Due to the special positions of U and Ni atoms in the UNi_2Al_3 structure, Bragg reflections can be split into two families:

$$\text{for } h-k=3n \qquad F_M(h,k,l) = \mu^{\rm U} f^{\rm U}(h,k,l) + 2\mu^{\rm Ni} f^{\rm Ni}(h,k,l) \tag{3}$$

$$\text{for } h-k\neq 3n \qquad F_M(h,k,l) = \mu^{\rm U} f^{\rm U}(h,k,l) - \mu^{\rm Ni} f^{\rm Ni}(h,k,l). \tag{4}$$

The solid lines in figure 3 correspond to calculated values for these different reflections.

As already suggested by MaxEnt, the strongest moment is found on the U site (8.80(6) and 8.65(6) $\times\ 10^{-3}\ \mu_B\ T^{-1}$ for the U^{4+} and U^{3+} configurations, respectively). The orbital-to-spin-moment ratios for this atom (deduced from the refined C_2-values) are in good agreement within error bars with the theoretical ones calculated in the intermediate-coupling scheme for either U^{4+} or U^{3+} (cf. table 3).

The small contribution on the Ni site suggested by the MaxEnt approach is confirmed by the refinements. It amounts to 0.35(4) $\times\ 10^{-3}\ \mu_B\ T^{-1}$ whatever the uranium valence state.

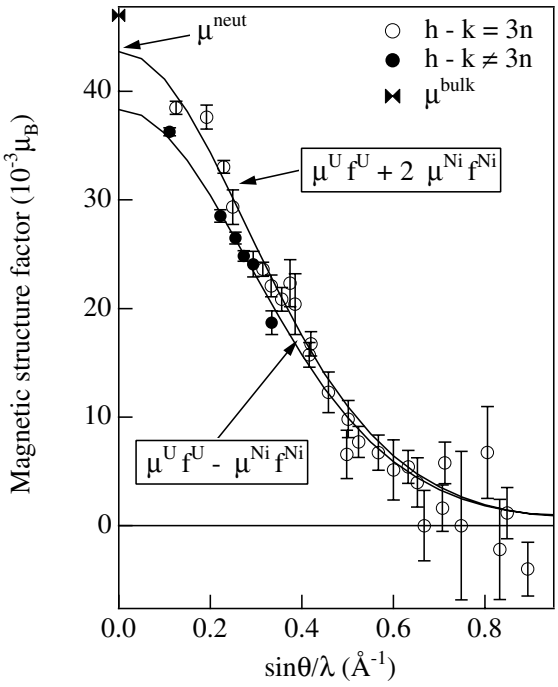

Figure 3. Magnetic structure factor versus $(\sin\theta)/\lambda$ for UNi_2Al_3 at 4.6 T and 100 K assuming a U^{4+} configuration. Empty and full points are experimental data. The solid lines correspond to calculated values. The bulk magnetization, $\mu^{\rm bulk}$, is also reported.

The sum of the U and Ni contributions in the unit cell, $\mu^{\rm neut}$, reaches 9.50(10) or 9.35(10) $\times 10^{-3}$ μ_B T^{-1} assuming U^{4+} or U^{3+} configurations, respectively. The difference between this quantity and the bulk magnetic moment, $\mu^{\rm cond} = \mu^{\rm bulk} - \mu^{\rm neut}$ (with $\mu^{\rm bulk} = 10.2(1) \times 10^{-3}$ μ_B T^{-1}), can be ascribed to a small diffuse contribution parallel to the 5f moment.

3. X-ray magnetic circular dichroism at the $M_{4,5}$ edges in UNi_2Al_3

3.1. Background and experimental procedure

The x-ray magnetic circular dichroism technique is able to determine the expectation values $\langle L_z\rangle$ and $\langle S_z\rangle$, where L_z and S_z are the z-projections of respectively the orbital and the spin angular momentum of a given electronic shell for a given element. This technique relies on the fact that when a right- or a left-polarized x-ray beam impinges on a magnetic material, the absorptions are different. Using sum rules [23, 24] it is possible to connect this absorption difference to both $\langle L_z\rangle/n_h$ and $\langle L_z\rangle/\langle S_z^e\rangle$ with $\langle S_z^e\rangle \equiv \langle S_z\rangle + 3\langle T_z\rangle$, where S_z^e is the effective spin operator. $\langle T_z\rangle$ is the expectation value of the z-projection of the magnetic dipole operator of the shell of interest and n_h is the number of holes in this shell. The main difficulty in evaluating $\langle S_z\rangle$ arises in the determination of $\langle T_z\rangle$, since it generally differs from the free-ion value.

Absorption spectra have been measured at the ID12A beamline of ESRF (European Synchrotron Radiation Facility, France), which is dedicated to polarization-dependent x-ray absorption studies [25, 26]. Indeed, the helical undulator Helios-II source provides high flux, high circular polarization rate (about 0.97) and tunable helicity of the incoming beam.

Since we were interested in the 5f-electron magnetism, the XMCD measurements were performed at the $M_{4,5}$ edges of uranium (3726 and 3551 eV, respectively) where the $3d_{3/2,5/2} \rightarrow 5f$ transitions are involved. The incident energies have been selected by a double-Si(111)-crystal monochromator, which induces a decrease of the beam circular polarization rate down to 0.35 at the energy of the M_5 edge and 0.45 at the M_4 one [27].

Since direct absorption measurements are impossible with thick samples containing uranium, the best detection technique for bulk property studies is fluorescence-yield detection. The main drawback of this method is the self-absorption effect. A correction of the fluorescence data to obtain the absorption coefficient is then required. This correction procedure can be found in several references, such as [28–30].

The experimental geometry of the measurement is presented in figure 4. The two sets of spectra needed for the dichroism were recorded by switching the handedness of the circular polarization. The external applied-field direction was within the ($\boldsymbol{a}$, $\boldsymbol{b}$) plane, in which the magnetization is isotropic, making a 15° angle with the $\boldsymbol{a}$-axis. Previous study on HFS [31,32] showed that XMCD measurements are possible in the paramagnetic state of antiferromagnets if sufficient bulk magnetization is induced by a high magnetic field. Therefore, we have chosen $B_{\mathrm{ext}} = 7$ T (produced by a superconducting cryomagnet) and $T = 100$ K in order to maximize the magnetic contribution.

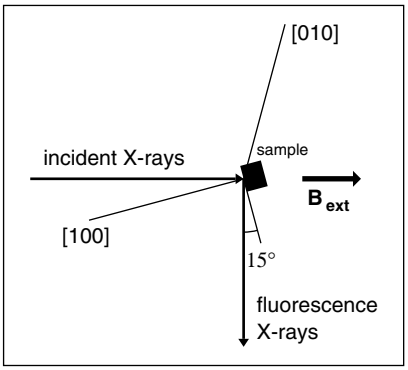

Figure 4. A schematic top view of the experiment. The $\boldsymbol{a}$- and $\boldsymbol{b}$-axes ([100] and [010]) are in the figure plane.

3.2. Results

In figure 5, the absorption spectra and associated dichroic signal are presented for the uranium M_4 edge. We did not manage to measure a reliable dichroism signal at the M_5 edge—which is expected to be extremely small. Due to these difficulties and considering the previous XMCD study performed on the parent compound UPd_2Al_3 [31] in which the dichroism area at M_5 was less than 10% of the M_4 one, we have assumed the XMCD at the M_5 edge in UNi_2Al_3 to be negligible†. Then, using the sum rules, the area of the absorption spectra at the $M_{4,5}$ edges and the XMCD area at the M_4 edge solely, we obtained $\langle L_z \rangle / (3n_h) = -2.5(3) \times 10^{-3}$ and $2\langle S_z^e \rangle / (3n_h) = 3.8(5) \times 10^{-3}$. We point out that the uncertainties indicated here take into account our assumption of a negligible XMCD signal at the M_5 edge. From $\langle L_z \rangle / (3n_h)$, we can calculate μ_L^{U} for either a U^{3+} or U^{4+} valence state. These values are reported in table 3.

† In all the available uranium XMCD data, the area of the M_5-edge dichroism signal is $\lesssim$10% of the M_4 one. See e.g. references [31,32] and references therein.

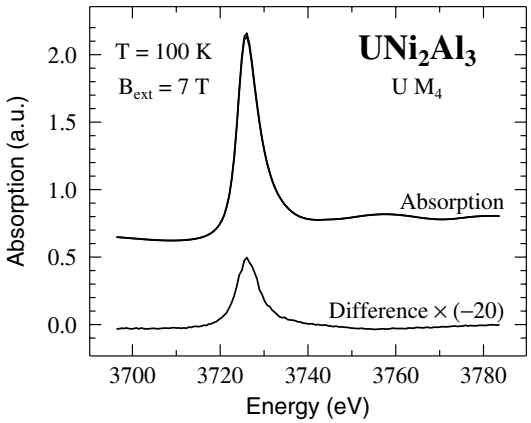

Figure 5. Absorption and dichroism spectra at the M_4 edge of uranium in UNi_2Al_3 at 100 K and 7 T. These spectra have been deduced from the fluorescence spectra, which have been corrected for self-absorption and for the energy dependence of the circular polarization rate of the monochromatic beam.

4. Discussion and comparison with UPd_2Al_3

The values μ_L^{U} obtained by the two techniques are in rather good agreement, whatever the assumed 5f configuration.

Since the value of $\langle T_z \rangle$ is necessary for estimating the spin magnetic moment with the XMCD technique, we choose to calculate this contribution, $\mu_S^{\mathrm{U}} = \mu^{\mathrm{U}} - \mu_L^{\mathrm{U}}$, by combining the 5f uranium magnetic moment μ^{U} deduced from polarized neutron data and the orbital 5f moment μ_L^{U} obtained from XMCD results. Since $\langle S_z^e \rangle$ is known from XMCD,

$$\Re_T \equiv \langle T_z \rangle / \langle S_z \rangle = (\langle S_z^e \rangle / \langle S_z \rangle - 1)/3$$

can then be calculated and compared to the free-ion values (cf. table 3).

The main difference between UNi_2Al_3 and UPd_2Al_3 arises from the small contribution on the Ni site (7(1)% of the bulk magnetization) observed in UNi_2Al_3 where no such contribution has been detected on the Pd site in UPd_2Al_3.

A diffuse moment parallel to the 5f one is observed in both compounds with however a stronger relative amplitude in the Pd counterpart (7(2)% and 13(2)% of the bulk magnetization for Ni and Pd compounds, respectively).

In the case of UNi_2Al_3, the ratios $\Re_L$ obtained from neutron data agree with the free-ion values whatever the assumption is regarding the uranium valence state. In contrast, for UPd_2Al_3, this ratio is found to be systematically lower, in particular for the U^{4+} hypothesis. According to Lander *et al* [33], this seems to indicate a stronger hybridization compared to that of the nickel compound. Since a magnetization density is found on the Ni site and not on the Pd one, this hybridization in UPd_2Al_3 would be more of $U_{5f} \rightarrow U_{6d}$ than of $U_{5f} \rightarrow T_d$ character. For both compounds, due to experimental uncertainties, no conclusion can be drawn from neutron data concerning the valence state of uranium. On the other hand, the $\Re_T$-ratios deduced from XMCD measurements seem to favour a U^{3+} hypothesis for the Pd compound, whereas the large error bars due to the weakness of the dichroism signal forbid any such conclusion for UNi_2Al_3.

5. Conclusions

We have presented polarized neutron and XMCD measurements at the uranium $M_{4,5}$ edges in the paramagnetic phase of UNi_2Al_3. From these measurements we have evidenced a magnetic moment on the nickel site and a diffuse contribution parallel to the 5f moment, and deduced the 5f orbital and spin contributions on the U atom. The orbital moment values, determined independently by the two techniques, have been found to be in good agreement.

The comparison of these results with the ones previously obtained for UPd_2Al_3 has led us to the following conclusions.

The uranium contribution is roughly the same in the two compounds and amounts to 86(2)% of the bulk magnetization. In UNi_2Al_3, half of the remaining 14% is carried by the Ni atom, the other half being ascribed as a diffuse contribution. In UPd_2Al_3, no magnetization is found on the Pd site and the diffuse contribution is double. This seems to indicate a larger U_{5f}–U_{6d} hybridization in this compound and this conclusion is also supported by the values obtained for the orbital-to-spin-moment ratio being systematically lower than the free-ion values [33]. On the other hand, the magnetization distribution observed on the Ni site could be explained by a stronger U_{5f}–T_d hybridization in UNi_2Al_3 in agreement with the LDA calculations [7].

Finally, we note that the existence of a magnetization density at the Ni and Pd sites could also be checked by performing XMCD experiments at the Ni, Pd ($L_{2,3}$) edges.

Acknowledgment

The authors are very grateful to Dr R Ballou for his kind help in some of the magnetization measurements performed at the CNRS.

References

[1] Metoki N, Haga Y, Koide Y and Onuki Y 1998 *Phys. Rev. Lett.* **80** 5117
[2] Bernhoeft N, Sato N, Roessli B, Aso N, Hiess A, Lander G H, Endoh Y and Komatsubara T 1998 *Phys. Rev. Lett.* **81** 4244
[3] Geibel C, Thies S, Kaczorowski D, Mehner A, Grauel A, Seidel B, Ahlheim U, Helfrich R, Petersen K, Bredl C D and Steglich F 1991 *Z. Phys.* B **83** 305
[4] Steglich F, Ahlheim U, Böhm A, Bredl C D, Caspary R, Geibel C, Grauel A, Helfrich R, Köhler R, Lang M, Mehner A, Modler R, Schank C, Wassilew C, Weber G, Assmus W, Sato N and Komatsubara T 1991 *Physica* C **185–189** 379
[5] Grauel A, Böhm A, Fisher H, Geibel C, Köhler R, Modler R, Schank C, Steglich F and Weber G 1992 *Phys. Rev.* B **46** 5818
[6] Geibel C, Böhm A, Caspary R, Gloos K, Grauel A, Hellman P, Modler R, Schank C, Weber G and Steglich F 1993 *Physica* B **186–188** 188
[7] Sticht J and Kübler J 1992 *Z. Phys.* B **87** 299
[8] Knöpfle K, Mavromaras A, Sandratskii L M and Kübler J 1996 *J. Phys.: Condens. Matter* **8** 901
[9] Sandratskii L M, Kübler J, Zahn P and Mertig I 1994 *Phys. Rev.* B **50** 15 834
[10] Paolasini L, Paixão J A, Lander G H, Delapalme A, Sato N and Komatsubara T 1993 *J. Phys.: Condens. Matter* **5** 8905
[11] Geibel C, Schank C, Thies S, Kitazawa H, Bredl C D, Böhm A, Rau M, Grauel A, Caspary R, Helfrich, Ahlheim U, Weber G and Steglich F 1991 *Z. Phys.* B **84** 1
[12] Krimmel A, Fisher P, Roessli B, Maletta H, Geibel C, Schank C, Grauel A, Loidl A and Steglich F 1992 *Z. Phys.* B **86** 161
[13] Sato N, Koga N and Komatsubara T 1996 *J. Phys. Soc. Japan* **65** 1555
[14] Nathans R, Pigott M T and Shull C G 1958 *J. Phys. Chem. Solids* **6** 38
[15] Wolfers P 1990 *J. Appl. Crystallogr.* **23** 554
[16] Becker P J and Coppens P 1974 *Acta Crystallogr.* A **30** 129

[17] Papoular R J and Gillon B 1990 *Europhys. Lett.* **13** 429
[18] Papoular R J, Zheludev A, Ressouche E and Schweizer J 1995 *Acta Crystallogr.* A **51** 295
[19] Zheludev A, Papoular R J, Ressouche E and Schweizer J 1995 *Acta Crystallogr.* A **51** 450
[20] Balcar E and Lovesey S W 1989 *Theory of Magnetic Neutron and Photon Scattering* (Oxford: Oxford University Press) ch 2
[21] Brown P J 1992 *International Tables for Crystallography* vol C, ed A J C Wilson (Dordrecht: Kluwer–Academic) p 391
[22] Brown P J and Matthewman C J 1993 *The Cambridge Crystallography Subroutine Library, Rutherford Appleton Laboratory Report* RAL-93-009
[23] Thole B T, Carra P, Sette F and van der Laan G 1992 *Phys. Rev. Lett.* **68** 1943
[24] Carra P, Thole B T, Altarelli M and Wang X 1993 *Phys. Rev. Lett.* **70** 694
[25] Goulon J, Brookes N B, Gauthier C, Goedkoop J, Goulon-Ginet C, Hagelstein M and Rogalev A 1995 *Physica* B **208+209** 199
[26] Gauthier C, Goulon G, Feite S, Moguiline E, Braicovich L, Brookes N B and Goulon J 1995 *Physica* B **208+209** 232
[27] Malgrange C, Carvalho C, Braicovich L and Goulon J 1991 *Nucl. Instrum. Methods* A **308** 390
[28] Jaklevic J, Kirby J A, Klein M P, Robertson A S, Brown G S and Eisenberger P 1977 *Solid State Commun.* **23** 679
[29] Eisebitt S, Böske T, Rubensson J E and Eberhardt W 1993 *Phys. Rev.* B **47** 14 103
[30] Dalmas de Réotier P, Sanchez J P, Yaouanc A, Finazzi M, Sainctavit Ph, Krill G, Kappler J P, Goedkoop J, Goulon J, Goulon-Ginet C, Rogalev A and Vogt O 1997 *J. Phys.: Condens. Matter* **9** 3291
[31] Yaouanc A, Dalmas de Réotier P, van der Laan G, Hiess A, Goulon J, Neumann C, Lejay P and Sato N 1998 *Phys. Rev.* B **58** 8793
[32] Dalmas de Réotier P, Yaouanc A, van der Laan G, Kernavanois N, Sanchez J P, Smith J L, Hiess A, Huxley A and Rogalev A 1999 *Phys. Rev.* B **60** 10 606
[33] Lander G H, Brooks M S S and Johanson B 1991 *Phys. Rev.* B **43** 13 672
[34] van der Laan G and Thole B T 1996 *Phys. Rev.* B **53** 14 458